

Gaze-guided Hand-Object Interaction Synthesis: Dataset and Method

Jie Tian, Ran Ji, Lingxiao Yang, Suting Ni, Yuexin Ma, Lan Xu, Jingyi Yu *IEEE Fellow*, Ye Shi, Jingya Wang

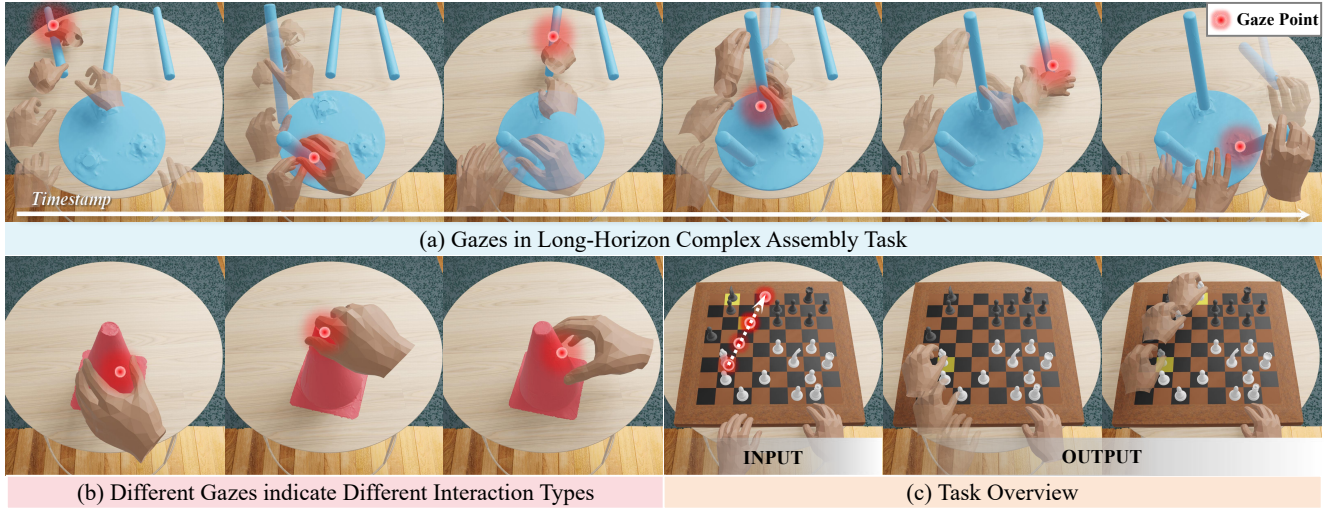


Figure 3. Gaze plays a crucial role in hand-object interaction tasks. The subfigure (a) illustrates how gaze helps coordinate the hands, objects, and brain during complex table assembly. The subfigure (b) shows how gaze affects attention allocation and grasp strategies. Building on these observations, we introduce the gaze-guided hand-object interaction synthesis task, as depicted in the subfigure (c), which uses gaze data as input to generate hand-object interactions that align with human intentions.

Abstract—Gaze plays a crucial role in revealing human attention and intention, particularly in hand-object interaction scenarios, where it guides and synchronizes complex tasks that require precise coordination between the brain, hand, and object. Motivated by this, we introduce a novel task: **Gaze-Guided Hand-Object Interaction Synthesis**, with potential applications in augmented reality, virtual reality, and assistive technologies. To support this task, we present **GazeHOI**, the first dataset to capture simultaneous 3D modeling of gaze, hand, and object interactions. This task poses significant challenges due to the inherent sparsity and noise in gaze data, as well as the need for high consistency and physical plausibility in generating hand and object motions. To tackle these issues, we propose a stacked gaze-guided hand-object interaction diffusion model, named **GHO-Diffusion**. The stacked design effectively reduces the complexity of motion generation. We also introduce **HOI-Manifold Guidance** during the sampling stage of **GHO-Diffusion**, enabling fine-grained control over generated motions while maintaining the data manifold. Additionally, we propose a **spatial-temporal gaze feature encoding** for the diffusion condition and select diffusion results based on consistency scores between gaze-contact maps and gaze-interaction trajectories. Extensive experiments highlight the effectiveness of our method and the unique contributions of our dataset. More details in <https://takiee.github.io/gaze-hoi/>.

Index Terms—Hand-object interaction, gaze, dataset, motion generation

I. INTRODUCTION

Gaze serves as a significant behavioral signal, directly reflecting human attention distribution and cognitive processes [1]–[3]. Extensive research has been conducted on gaze, including gaze estimation [4]–[10] and human action prediction based on gaze [11]–[15]. While these studies have explored gaze in various applications, they have primarily focused on broad human motions, with limited attention given to hand

movements and detailed dynamic interactions within fine-grained environments. Furthermore, gaze is particularly crucial in hand-object interactions, as it reveals “when, where, and how” the user interacts with the object. Figure 3(a) illustrates how gaze supports long-horizon synthesis for complex tasks, while Figure 3(b) shows that gaze indicates how humans interact with objects using different parts and interaction types. By effectively identifying objects and areas of focus, gaze enables the seamless integration of human intentions and motions, ensuring precise coordination and consistency between the brain, hands, and objects. This coordination is essential for executing complex interactions, such as grasping, manipulating, or positioning objects, thereby enhancing both the efficiency and accuracy of these motions.

Motivated by this, we propose a novel task: **Gaze-guided Hand-Object Interaction Synthesis**, as shown in Figure 3(c). This task leverages gaze to naturally generate motions that align with human intent, eliminating the need for additional textual annotations or motion references. This approach is particularly well-suited for integration into VR/AR environments and assistive technologies. For example, in VR/AR settings, gaze-guided technology allows users to interact with virtual objects more intuitively by accurately predicting their intentions without the need for physical controllers. Additionally, it benefits individuals with disabilities by allowing them to control interactions through eye movements, enhancing their ability to express intentions and perform tasks

Existing hand-object datasets [16]–[25] are limited to interactions between hands and objects, often neglecting gaze information. To fill this gap, we introduce **GazeHOI**, the first dataset that simultaneously integrates 3D modeling of gaze, hand, and object interactions. **GazeHOI** presents significant challenges

due to the diverse shapes and sizes of objects, ranging from small items like chess pieces to larger, assemblable furniture. Additionally, the dataset covers a wide range of complex tasks, including repositioning objects, selecting specific targets within cluttered environments, organizing disordered items, and assembling furniture.

However, leveraging gaze data for generating hand and object motions presents significant challenges. The inherent sparsity and noise in gaze data make it difficult to reliably capture and interpret user intentions. Additionally, achieving high consistency and physical plausibility in the generated motions is a complex task, as it requires accurate synchronization between gaze input and corresponding hand-object interactions. To address these challenges, we propose a novel approach: a stacked gaze-guided hand-object interaction diffusion model, named GHO-Diffusion. We decouple the task into two stages: gaze-activated object dynamics synthesis and object-driven hand kinematic synthesis. Moreover, we introduce HOI-Manifold Guidance during the sampling stage of GHO-Diffusion. This technique allows for fine-grained control over the generated motions, ensuring they remain within the data manifold and adhere to the natural constraints of hand-object interactions. Additionally, to further leverage gaze information, we propose a spatial-temporal gaze feature encoding approach for the diffusion condition. This method captures both spatial and temporal aspects of gaze data, enhancing the diffusion process with detailed representations of gaze interactions. We also select diffusion results based on consistency scores between gaze-contact maps and gaze-interaction trajectories. Our contributions can be summarized as follows:

1) A Novel Task and Dataset. We introduce the novel task of gaze-guided hand-object interaction synthesis, which utilizes gaze to generate natural interaction motions that align with human intent. To support this task, we present GazeHOI, the first dataset incorporating gaze information for hand-object interactions.

2) GHO-Diffusion Model. We develop the Gaze-guided Hand-Object interaction Diffusion model, GHO-Diffusion, which employs stacked diffusion models to reduce the complexity of motion modeling. Furthermore, we integrate the HOI-Manifold Guidance during the inference phase of GHO-Diffusion, providing fine-grained control over generated motions while maintaining the data distribution learned by the diffusion model.

3) Gaze-Guided Feature Encoding and Motion Selection. We propose a gaze-guided spatial-temporal feature encoding as the diffusion condition, coupled with a mechanism to select diffusion results based on consistency scores between gaze-contact maps and gaze-interaction trajectories. This approach ensures that the generated motions are precisely aligned with the given gaze input.

II. RELATED WORK

A. Gaze for Perception

Gaze serves as a key behavioral signal, revealing intentional cues and providing insights into attention, interest, and cognitive processes. Early research, constrained by the expense

TABLE I
COMPARISON OF GAZEHOI WITH EXISTING GAZE DATASETS

	Gaze	Object pose	Hand pose
MoGaze [11]	✓	✓	×
GIMO [12]	✓	×	✓
ActionSense [13]	✓	×	✓
MECCANO [14]	✓	×	×
HoloAssist [28]	✓	×	✓
ADT [29]	✓	✓	×
EgoBody [30]	✓	×	✓
GazeHOI	✓	✓	✓

and accuracy limitations of gaze tracking equipment, focused on estimating gaze from third-person perspective images or videos [4]–[10] to predict human attention regions. With advancements in gaze tracking technology [27], acquiring accurate gaze information has become more accessible, leading to the emergence of diverse datasets [11]–[15], [28]–[30] annotated with gaze information. Recent studies have expanded from simply capturing gaze to leveraging its contextual richness, such as inferring vehicle ego-trajectory [15] or predicting interaction action labels [31]. However, existing gaze-motion datasets [11]–[13], [28]–[30] and methods largely overlook the crucial relationship between gaze and hand-object interaction—key for fine-grained intent inference and enhancing realism in applications like VR. From a dataset perspective, current datasets either lack hand pose capture [11], [29] or object pose capture [12], [13], [28], [30] as shown in Table I. From a task perspective, most focus on human motion prediction [12], [32], [33], neglecting the precision required for hand-object interactions, such as realistic contact, penetration avoidance, and plausible physical dynamics. Existing human motion prediction methods also rely heavily on historical motion sequences, using gaze data as auxiliary input within gaze-motion fusion encoders. These approaches fail to fully exploit the spatial relationships between gaze and objects and the temporal dynamics of gaze in hand-object interactions. To address these gaps, we present the first dataset to simultaneously capture 3D gaze, hand, and object interactions, with the novel task of gaze-guided hand-object interaction motion synthesis from an initial state, without relying on historical motions. To effectively capture the intentionality inherent in gaze, we design a gaze-guided spatial-temporal feature encoding as diffusion condition and develop a mechanism to select the diffusion results based on consistency scores computed between gaze-contact maps and gaze-interaction trajectories.

B. Hand-Object Interaction Dataset

Numerous datasets [16]–[25] dedicated to hand-object interactions have been developed to facilitate the capture of hand and object poses and to deepen our understanding of these interactions, as shown in Table II. Most datasets only capture simple interaction patterns, like grasping and moving, which is common but not comprehensive enough. HOI4D [20] and ARCTIC [21] explore the interaction of articulated objects. TACO [22] and OakInk2 [25] captures scenes of simultaneous interactions with multiple objects. Furthermore, existing datasets focus exclusively on the relationship between hands and objects, neglecting the role of gaze. To address

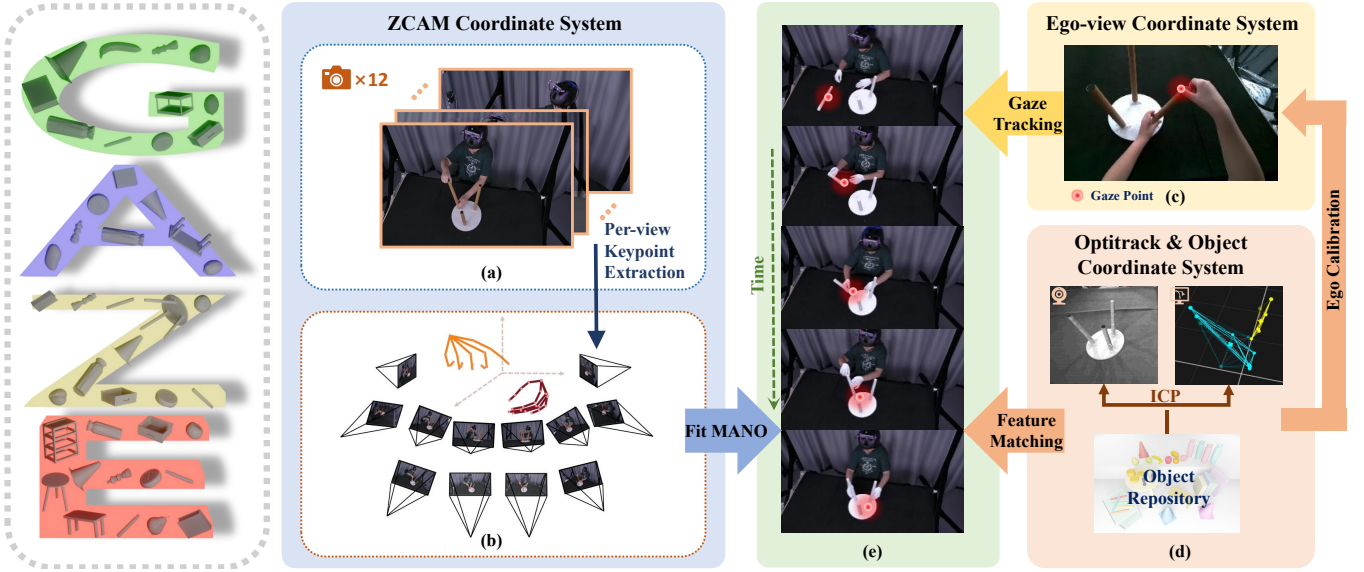


Fig. 4. Automatic data processing pipeline. (a) displays 12-view images from the raw video. (b) uses mediapipe [26] to get hand 2D joints and triangulation to obtain the 3D joints. (c) shows the ego view with a gaze point. (d) illustrates the objects acquired by the scanner and the marker tracking process. (e) shows the result of hand-object motion.

TABLE II
COMPARISON OF GAZEHOI WITH EXISTING 4D HAND-OBJECT INTERACTION DATASETS.

	Gaze	Ego	Multi-obj	Complex	#views	#images
HO-3D [16]	×	×	×	×	1-4	78K
DexYCB [17]	×	×	×	×	8	582K
H2O [18]	×	✓	×	×	5	571K
OakInk [19]	×	×	×	×	4	230K
HOI4D [20]	×	✓	×	×	2	2.4M
ARCTIC [21]	×	✓	×	×	9	2.1M
TACO [22]	×	✓	✓	✓	13	5.2M
OAKINK2 [25]	×	✓	✓	✓	4	4.01M
GazeHOI	✓	✓	✓	✓	13	3.2M

this gap, we introduce a comprehensive egocentric dataset enriched with detailed gaze annotations. This dataset captures the dynamics of hand-object interactions across a wide range of tasks, from arranging chess pieces to assembling furniture — scenarios not covered in existing datasets. Our goal is to bridge the shortcomings of current datasets by providing a resource that reflects the complexity of real-world interactions and emphasizes the importance of gaze in predicting human intent and managing multi-object manipulation.

C. Hand-Object Motion Synthesis

In the field of hand-object motion synthesis, prior efforts have mainly centered on frame-wise generation [34]–[37]. For dynamic hand-object interaction, previous methods typically rely on motion references, such as trajectories [38]–[43] or grasp references [44], or only focus on approaching stage [45], [46]. Recently, there are several works that study the hand-object interaction generation directly based on text [47], [48], significantly reducing the reliance on specific conditions. Building on advancements in 3D gaze acquisition technology, our work further relaxes these constraints by generating hand-object interactions directly from gaze data. Compared to text, gaze-based generation aligns more closely with the user’s intent, resulting in more intuitive hand-object interactions.

III. GAZEHOI DATASET

Existing datasets primarily focus on the interaction between hands and objects, overlooking the crucial role of gaze. However, a comprehensive understanding of interaction requires coordinated hand-eye-object cooperation. To address this gap, we present GazeHOI, the first interaction dataset that simultaneously incorporates 3D modeling of gaze, hand, and object interactions. GazeHOI encompasses 237K frames with an average duration of 19.1 seconds and 2-4 objects per sequence, further divisible into 1378 subsequences. We collect 33 different objects with various shape and size, the smallest of which is a chess piece with a height of 7cm and a mere diameter of 2cm. Each sequence is accompanied by a task-level description, which varies in complexity, and includes repositioning objects to another location, selecting specific targets from cluttered environments, organizing items from disarray into order, and assembling furniture. This rich variety aims to provide comprehensive insights into the intricate dynamics of interactive behaviors.

A. Dataset Hardware Setup

To construct the GazeHOI dataset, we developed a data collection platform encompassing a $1.6\text{m} \times 1.2\text{m}$ area, equipped with a multi-camera system. This platform comprises four distinct equipment systems. The ZCAM system includes 12 ZCAM E2 cameras that have been synchronized through hardware, capturing RGB signals at a resolution of 3840×2160 at 30fps, which are utilized for subsequent hand pose acquisition. The Optitrack system consists of 8 hardware-synchronized Optitrack px13W cameras, which use infrared to capture the positions of reflective markers at a frame rate of 120fps, facilitating the tracking of object poses. The Scanner system, comprising two EinScan Pro 2X and EinScan SE scanners, is dedicated to collecting geometric information about objects. The Ego system, primarily aimed at gathering gaze data, employs a Pupil Core connected to a RealSense D455,

simultaneously recording gaze information along with RGBD data from an ego-centric perspective. We devise a sophisticated workflow to achieve coordinate system registration among the 4 equipment systems. Each system is tasked with collecting specific types of data, and we have devised a sophisticated workflow to achieve coordinate system registration among the 4 equipment systems through reflective markers. We attached eight 10mm diameter markers on the surface of the RealSense and scanned it to obtain its 3D model. By annotating the position of each marker in every RGB viewpoint and triangulating these positions, we could ascertain the location of markers within each system, thereby aligning the coordinate systems of multiple devices.

B. Data Collection

We recruited 10 volunteers (5 males and 5 females) to assist us in data collection. Before the collection process, we provided the participants with a comprehensive script that detailed the tasks they were required to complete. For each task, participants were asked to perform multiple iterations. Consequently, individuals often scan their surroundings to gain a preliminary understanding of the environment before executing the action in unfamiliar settings, leading to longer gaze duration for task-relevant objects. As familiarity with the scene increases, the gaze becomes more focused, and the gaze duration correspondingly decreases. This approach ensures the authenticity and naturalness of the gaze data, accurately reflecting real-world gaze behavior.

C. Data Annotation

1) *3D Hand Pose*: 12 synchronized ZCAM cameras afford us an exhaustive 3D perspective of the hand, as shown in Figure 4(a). By harnessing the capabilities of MediaPipe [26], we execute 2D hand keypoint tracking across individual video frames. Through the application of triangulation algorithms, we transition the 2D keypoints observed from disparate views to their respective 3D coordinates in global space shown in Figure 4(b). Subsequently, we derive the corresponding MANO [49] parameters through an optimization process that accounts for joint alignment, realistic anatomical constraints.

2) *Object 6D Pose*: We focus on rigid objects, enabling us to determine the 6D poses by tracking reflective markers attached to the surfaces via Optitrack. We strategically placed at least eight 3mm markers on each object to minimize interference with natural interactions and prevent occlusions that could affect marker recognition. Before data collection, we employ a 3D scanner to capture the precise geometry of the object surfaces. The Iterative Closest Point algorithm is used to convert the reflection points detected by OptiTrack into the 6D pose of the object. Figure 4(d) shows our object repository acquired by scanner and tracking process.

3) *Gaze Acquisition*: The eye tracker Pupil Core provides 3D gaze data from an egocentric viewpoint, requiring us to perform ego calibration to unify gaze, hand, and object data within a single coordinate system. Similar to object tracking, we attach markers to the ego camera to achieve this calibration. We also apply post-processing techniques, such as removing gaze data with very short durations and smoothing, to reduce

noise and enhance the quality of the gaze data. Figure 4(c) shows the gaze during data collection.

IV. METHOD

A. Problem Definition

We define a gaze-consistent hand-object interaction sequence of length l as $\mathbf{S} = \langle \mathbf{G}, \mathbf{H}, \mathbf{O} \rangle$, where $\mathbf{G} = \{\mathbf{g}_i\}_{i=1}^l$ represents the gaze sequence, with each $\mathbf{g}_i \in \mathbb{R}^3$ denoting the gaze point in the i -th frame. $\mathbf{H} = \{\mathbf{h}_l^i, \mathbf{h}_r^i\}_{i=1}^l$ denotes the hand motion sequences, comprising left-hand motions \mathbf{h}_l^i and right-hand motions \mathbf{h}_r^i . Each hand motion $\mathbf{h}^i = \{\mathbf{R}_h^i, \mathbf{T}_h^i, \theta^i, \beta\} \in \mathbb{R}^{61}$ follows the MANO [49] parameterization, where \mathbf{R}_h^i is the rotation, \mathbf{T}_h^i is the translation, θ^i represents the pose and β represents shape parameters; $\mathbf{O} = \{\mathbf{o}^i\}_{i=1}^l$ is the object motion sequence, where each $\mathbf{o}^i = \{\mathbf{R}_o^i, \mathbf{T}_o^i\} \in \mathbb{SE}(3)$ denotes the object's pose, with \mathbf{R}_o^i as the rotation and \mathbf{T}_o^i as the translation. Additionally, we define the object geometry as a set of vertices $\mathbf{P}_o = \{\mathbf{p}_o^n\}_{n=1}^N \in \mathbb{R}^{N \times 3}$, where N represents the number of object vertices. Given the input $\mathcal{I} = \{\mathbf{G}, \mathbf{h}_l^1, \mathbf{h}_r^1, \mathbf{o}^1, \mathbf{P}_o\}$, our objective is to derive a subsequent hand-object interaction sequence $\langle \mathbf{H}, \mathbf{O} \rangle$ that is not only consistent with the gaze but also exhibits natural and realistic interactions between the hand and the object.

B. GHO-Diffusion: Gaze-guided Hand-Object Diffusion

GHO-Diffusion decouples the complex hand-object interaction into two stacked diffusion stages, Object Dynamics Synthesis with Spatial-Temporal Gaze Encoding and Hand Kinematic Synthesis with HOI-Manifold Guidance as shown in Figure 5(a). This decoupling strategy reduces modeling complexity while effectively capturing both global spatial-temporal positioning and the intricate details of hand-object interaction motions.

The diffusion model contains a fixed forward process $q(\mathbf{x}_t | \mathbf{x}_0) = \mathcal{N}(\sqrt{\alpha_t} \mathbf{x}_0, (1 - \alpha_t) \mathbf{I})$ which gradually adds Gaussian noise to clean data \mathbf{x}_0 until it becomes pure noise $\epsilon \sim \mathcal{N}(\mathbf{0}, \mathbf{I})$ and train a denoiser $p_\theta(\mathbf{x}_t, t, \mathbf{c})$ to gradually denoise $\mathbf{x}_T \sim \mathcal{N}(\mathbf{0}, \mathbf{I})$ to generate \mathbf{x}_0 in the reverse process. Instead of predicting ϵ_t at each time step t , we follow MDM [50] to predict $\hat{\mathbf{x}}_0$ and optimizing $p_\theta(\mathbf{x}_t, t, \mathbf{c})$ using the simple objective function:

$$\mathcal{L}_{\text{simple}} = \mathbb{E}_{\mathbf{x}_0 \sim q(\mathbf{x}_0 | \mathbf{c}), t \sim [1, T]} \|\mathbf{x}_0 - p_\theta(\mathbf{x}_t, t, \mathbf{c})\|_2^2. \quad (1)$$

1) *Stage-1: Object Dynamics Synthesis with Spatial-Temporal Gaze Encoding*: The gaze point locations are closely related to the object surface vertices, and since object motions have fewer degrees of freedom compared to hand motions, so we generate the object motions first. Gaze is a sparse and noisy signal, making it challenging to encode effectively. Drawing inspiration from GIMO [12], we design a gaze-guided spatial-temporal feature encoding module for object diffusion. We define \mathbf{f}_o^k as the k -th local per-point object spatial feature extracted by PointNet++ [51]. Then according to the spatial relationship between gaze and object points, we can calculate gaze spatial feature:

$$\mathbf{f}_g = \|\mathbf{G} - \mathbf{P}_o^{k*}\|^{-1} \mathbf{f}_o^{k*}, \quad (2)$$

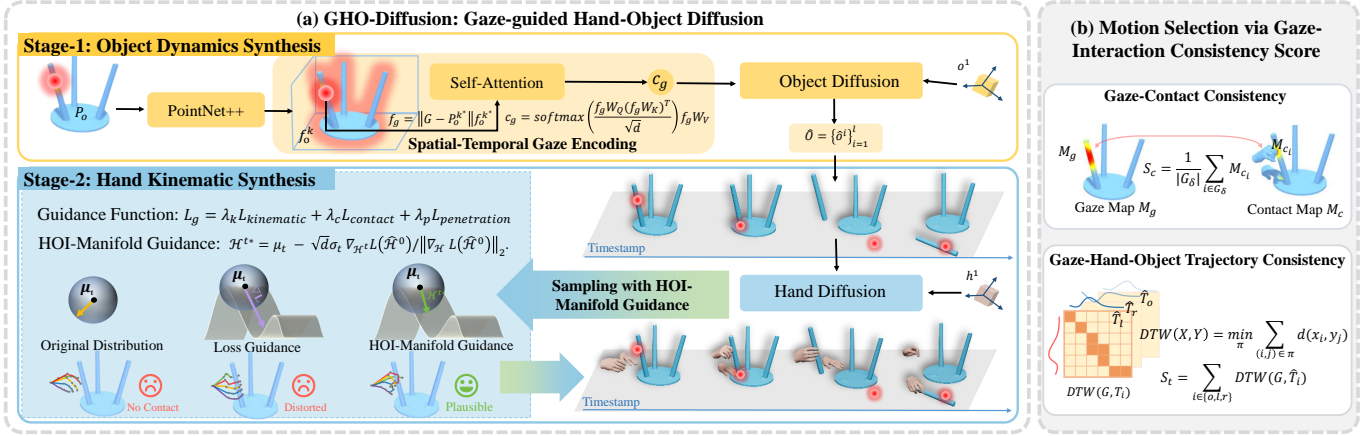


Fig. 5. Pipeline overview. The subfigure (a) illustrates the stacked framework of the gaze-guided hand-object interaction diffusion model, GHODiffusion. The subfigure (b) shows the gaze-interaction consistency score for motion selection.

where $k^* = \arg \min_{k=1}^N \| \mathbf{G} - \mathbf{P}_o^k \|$, representing the index of the object points that is closest to the gaze point in i -th frame. Subsequently, these spatial features are processed through a self-attention mechanism to extract the final spatial-temporal condition features:

$$\mathbf{c}_g = \text{softmax} \left(\frac{\mathbf{f}_g \mathbf{W}_Q (\mathbf{f}_g \mathbf{W}_K)^\top}{\sqrt{d}} \right) \mathbf{f}_g \mathbf{W}_V, \quad (3)$$

where \mathbf{W}_Q , \mathbf{W}_K , and \mathbf{W}_V are trainable weight matrices, and d is the dimension of the feature.

We leverage the gaze spatial-temporal features \mathbf{c}_g , along with the object geometry \mathbf{P} and initial object pose \mathbf{o}^1 as stage-1 diffusion condition and employ the objective function in Equation 4 as Stage-1 training loss to generate object motions $\hat{\mathbf{O}}$:

$$\mathcal{L}_{\text{stage1}} = \lambda_\alpha \mathcal{L}_{\text{simple}} + \lambda_\nu \mathcal{L}_{\text{verts}} + \lambda_t \mathcal{L}_{\text{trans}} + \lambda_s \mathcal{L}_{\text{smooth}}. \quad (4)$$

where $\mathcal{L}_{\text{simple}}$ is defined by Equation 1.

The object translation loss $\mathcal{L}_{\text{trans}}$ is defined as:

$$\mathcal{L}_{\text{trans}} = \sum_{i=1}^L \| \mathbf{T}_o^i - \hat{\mathbf{T}}_o^i \|_2, \quad (5)$$

which enforces a constraint on the object's position. The object vertices loss $\mathcal{L}_{\text{verts}}$ is defined as:

$$\mathcal{L}_{\text{verts}} = \sum_{i=1}^l \| (\mathbf{R}_o^i(\mathbf{P}) + \mathbf{T}_o^i) - (\hat{\mathbf{R}}_o^i(\mathbf{P}) + \hat{\mathbf{T}}_o^i) \|_2, \quad (6)$$

which enforces constraints on the object's surface geometry, promoting finer details and ensuring more precise alignment. The smoothness loss $\mathcal{L}_{\text{smooth}}$ is defined as:

$$\mathcal{L}_{\text{smooth}} = \| \mathcal{H}^{1:l} - \mathcal{H}^{0:l-1} \|_2, \quad (7)$$

which promotes the continuity and fluidity of the generated motion. By minimizing the difference between consecutive motion frames, this loss ensures that the generated object motion is smooth and avoids abrupt transitions between frames.

2) *Stage-2: Hand Kinematic Synthesis with HOI Guidance:* In this stage, we leverage the object motions $\hat{\mathbf{O}}$ generated in Stage-1 to synthesize the corresponding hand motions $\hat{\mathbf{H}}$ through a hand diffusion process. Hand motion synthesis presents greater complexity compared to object motion synthesis, primarily because hand movements are highly articulated and require more stringent constraints to ensure

natural and physically plausible outcomes. To address this, we adopt a canonicalized hand-object interaction representation: $\mathcal{H} = [\mathbf{J}, \mathbf{C}, \mathbf{F}, \mathbf{v}, \mathbf{a}]$. Here, hand poses are represented by joint positions \mathbf{J} , as neural networks typically learn translations more effectively than rotations. The contact flag $\mathbf{C} \in \mathbb{R}^{42}$ encodes the contact status of each joint, while the offset vector \mathbf{F} represents both hand-object and inter-hand spatial displacements. The velocity vector \mathbf{v} captures both linear and angular velocities for each hand, including their relative velocities, and the acceleration vector \mathbf{a} is similarly defined. To generate the hand motions $\hat{\mathbf{H}}$, we condition the synthesis on the generated object motions $\hat{\mathbf{O}}$, alongside object geometry \mathbf{P} and the initial hand pose \mathbf{h}^1 in Stage-2. For training, we employ the objective function from Equation 1 and introduce a bone length loss $\mathcal{L}_{\text{bone}}$ to maintain the structural integrity of the hand:

$$\mathcal{L}_{\text{stage2}} = \lambda_\beta \mathcal{L}_{\text{simple}} + \lambda_b \mathcal{L}_{\text{bone}}. \quad (8)$$

We define $\mathcal{B}(\cdot)$ as a function that calculates the bone lengths, taking the hand joints \mathbf{J} as input. The bone length loss $\mathcal{L}_{\text{bone}}$ is defined as:

$$\mathcal{L}_{\text{bone}} = \| \mathcal{B}(\mathbf{J}) - \mathcal{B}(\hat{\mathbf{J}}) \|_2. \quad (9)$$

Since hand diffusion effectively captures the overall distribution of hand-object interactions, it falls short of achieving precision in finer details, such as maintaining contact or avoiding penetrations. Therefore, we introduce HOI-Manifold Guidance to strengthen the physics constraint while preserving the original data distribution. We define three guidance functions from the perspective of Kinematic, Contact and Penetration.

a) *Hand-Object Kinematic Guidance:* We define redundancy parameters to enhance the reliability of hand motions while using only the hand joints for subsequent steps. The kinematic consistency guidance is designed for test-time adaptation, ensuring that the generated parameters remain consistent with those recalculated from the generated hand joints and object motion conditions. The loss function is as follow,

$$\mathcal{L}_{\text{kinematic}} = \| \hat{\mathbf{F}} - \tilde{\mathbf{F}} \|_2 + \| \hat{\mathbf{v}} - \tilde{\mathbf{v}} \|_2 + \| \hat{\mathbf{a}} - \tilde{\mathbf{a}} \|_2. \quad (10)$$

b) **Hand-Object Contact Guidance.**: We define a contact loss to minimize the distance between hand joints that are near the object’s surface but not yet in contact:

$$\mathcal{L}_{\text{contact}} = \frac{\sum_{i=1}^l d(\hat{\mathbf{J}}^i, \mathbf{P}_o^i) \cdot \mathbb{I}(d(\hat{\mathbf{J}}^i, \mathbf{P}_o^i) < \tau)}{\sum_{i=1}^l \mathbb{I}(d(\hat{\mathbf{J}}^i, \mathbf{P}_o^i) < \tau) + \epsilon}, \quad (11)$$

where $d(\hat{\mathbf{J}}^i, \mathbf{P}_o^i)$ is the closest distance between hand joint $\hat{\mathbf{J}}^i$ and object surface \mathbf{P}_o^i in i -th frame, τ is the contact threshold, \mathbb{I} is the indicator function, and ϵ is a small constant to prevent division by zero.

c) **Hand-Object Penetration Guidance.**: We calculate the dot product between the hand-object offset and the object surface normal to measure the penetration as follows,

$$\mathcal{L}_{\text{penetration}} = -\sum_{i=1}^l \min(0, \tilde{\mathbf{F}}^i \cdot \mathbf{n}^i + \eta), \quad (12)$$

where $\tilde{\mathbf{F}}^i$ is the recalculated offset vector from the generated hand joint $\hat{\mathbf{J}}^i$ to the object surface \mathbf{P}_o^i in i -th frame, \mathbf{n}^i is the normal vector at the closest object point in i -th frame, and η is a small constant that defines the acceptable penetration threshold. The overall guidance loss function is

$$\mathcal{L}_g = \lambda_k \mathcal{L}_{\text{kinematic}} + \lambda_c \mathcal{L}_{\text{contact}} + \lambda_p \mathcal{L}_{\text{penetration}}. \quad (13)$$

The naive guidance strategy, which directly adds the computed gradient $\nabla_{\mathcal{H}^t} \mathcal{L}(\mathcal{H}^0)$ to the sample, may misalign the final motions with the original data distribution, resulting in unnatural motions. Therefore, we aim to develop a guidance strategy that can achieve guidance targets while preserving the original distribution. Recently, a conditional diffusion model with the Spherical Gaussian constraint, named DSG [52] is proposed to offer larger, adaptive step sizes while preserving the original data distribution. However, its effectiveness has mainly been shown in image-generation tasks. Motivated by DSG, we introduce the Spherical Gaussian constraint to our sampling process, which ensures that the generated hand motion remains within the clean data distribution, resulting in natural and smooth hand motion generation.

We utilize closed-form solution \mathcal{H}^{t*} that enforces sampling in gradient descent direction while preserving \mathcal{H}^{t*} within noisy data distribution. This can ensure the generated \mathcal{H}^0 remaining within the clean data manifold:

$$\mathcal{H}^{t*} = \mu_t - \sqrt{d}\sigma_t \nabla_{\mathcal{H}^t} \mathcal{L}_g(\hat{\mathcal{H}}^0) / \|\nabla_{\mathcal{H}^t} \mathcal{L}_g(\hat{\mathcal{H}}^0)\|_2, \quad (14)$$

where σ_t represents the variance in time step t and d represents the data dimensions. To enhance generation diversity, we re-weight the direction of \mathcal{H}^{t*} and the sampling point \mathcal{H}^t similar to Classifier-free guidance:

$$\mathbf{D} = \mathcal{H}^t + w(\mathcal{H}^{t*} - \mathcal{H}^t), \quad (15)$$

$$\mathcal{H}^t = \mu_t + \sqrt{d}\sigma_t \mathbf{D} / \|\mathbf{D}\|, \quad (16)$$

where w represents the guidance rate that lies in $[0,1]$ and \mathbf{D} represents the weighted direction.

Since we represent the hand pose using hand joints, a post-optimization process is required to derive the corresponding MANO representation. We first calculate the global R by matching the actual MCP joint positions of the hand with its ideal position in the static state. The MCP joints are crucial

for determining the global orientation of the hand because they serve as the primary pivot points for finger movement and are centrally located, providing a stable reference for the overall hand pose. By matching these joints, we can accurately capture the hand’s global rotation, ensuring that the subsequent pose adjustments maintain anatomical correctness. Then we define a loss function $\mathcal{L}_{\text{joint}}$ as optimization target to align the generated joint \mathbf{J} with the joint calculated by manolayer $\mathcal{M}(\cdot)$,

$$\mathcal{L}_{\text{joint}} = \|\mathbf{J} - \mathcal{M}(\mathbf{H})\|_2. \quad (17)$$

To preserve the natural and realistic movement of the hand, we apply pose angle constraints at the end of each iteration. These constraints limit the rotation range of hand joints across different axes, with strict controls specifically on the Y-axis rotation of the MCP joints and the Z-axis rotation of the other joints.

C. Motion Selection via Gaze-Interaction Consistency Score

Motions generated by diffusion do not always fully conform to the gaze distribution. To address this, we explore gaze-interaction consistency from both a local and a global perspective, as shown in Figure 5(b). Locally, inspired by [3], we observe that areas receiving more visual attention are more likely to be contacted. So we compute the contact map $\mathbf{M}_c = e^{-\alpha \cdot d(\mathbf{P}_h, \mathbf{P}_o)}$ and gaze map $\mathbf{M}_g = e^{-\alpha \cdot d(\mathbf{G}, \mathbf{P}_o)}$ separately by the distance from hand vertices \mathbf{P}_h and gaze point \mathbf{G} to the object surface \mathbf{P}_o . The gaze-contact consistency score S_c is then calculated as follows,

$$S_c = \frac{1}{|\mathbf{G}_\delta|} \sum_{i \in \mathbf{G}_\delta} \mathbf{M}_{c_i}, \quad (18)$$

where \mathbf{G}_δ is the set of object points index that indicates where the distance $d(\mathbf{G}, \mathbf{P}_o) < \delta$, and $|\mathbf{G}_\delta|$ is the number of elements in this set. Globally, gaze-hand-object trajectories are expected to exhibit inherent relationships. To quantify this, we use Dynamic Time Warping (DTW) [53] to measure the gaze-hand-object trajectory similarity,

$$\text{DTW}(\mathbf{X}, \mathbf{Y}) = \min_{\pi} \sum_{(i,j) \in \pi} d(x_i, y_j), \quad (19)$$

where π is a warping path that aligns \mathbf{X} and \mathbf{Y} , and $d(x_i, y_j)$ is the distance between points x_i and y_j . The gaze-hand-object trajectory consistency score S_t is then defined as:

$$S_t = \text{DTW}(\mathbf{G}, \hat{\mathbf{T}}_l) + \text{DTW}(\mathbf{G}, \hat{\mathbf{T}}_r) + \text{DTW}(\mathbf{G}, \hat{\mathbf{T}}_o). \quad (20)$$

Then we combine S_c and S_t to select the top-k motions $\langle \hat{\mathbf{H}}, \hat{\mathbf{O}} \rangle$ that are most consistent with the gaze signals.

V. EXPERIMENTS

A. Data Split and Evaluation Metrics

We divided 1378 sequences into a training set with 1103 sequences and a test set comprising 275 sequences. To mitigate the model’s potential overfitting to object-specific traits, the test set exclusively includes objects not represented in the training set. Our evaluation metrics includes three parts: 1) motion consistency with gaze and accuracy by evaluating the

TABLE III
 QUANTITATIVE COMPARISON BETWEEN BASELINES AND OUR METHOD. THE GROUND TRUTH DIVERSITY IS 4.227 AND DIVERSITY RESULTS ARE BETTER IF THE METRIC IS CLOSER TO THE REAL DISTRIBUTION.

Methods	Accuracy			Grasp Quality		Generation		Human Perception	
	MPVPE ↓	FOL ↓	MPJPE ↓	CF↑	PD ↓	FID ↓	Diversity ↑	GMC↑	IN↑
MDM*	146.8	228.0	166.6	62.55	2.52	0.071	4.174	3.70	3.40
Text2HOI*	325.0	327.1	258.1	59.64	2.51	0.719	4.188	2.95	2.50
OMOMO*	-	-	161.2	62.61	2.49	0.051	4.121	4.15	4.05
Ours	117.4	146.5	144.8	68.10	2.46	0.044	4.217	4.75	4.60

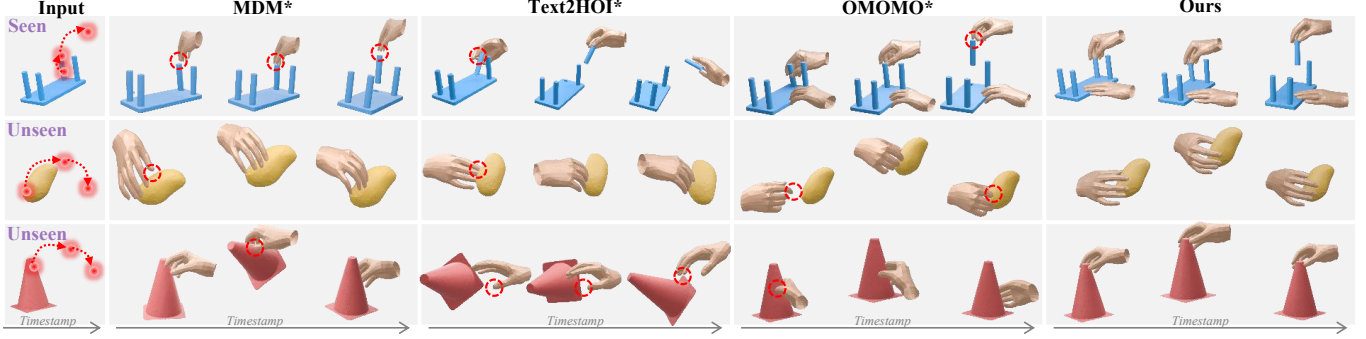


Fig. 6. Qualitative results between baseline methods and our method.

hand Mean Per Joint Position Error (MPJPE), object Mean Per Vertex Position Error (MPVPE), and the Final Object Location (FOL); 2) the stability and realism of hand-object interactions using the Contact Frame radio (CF) and the Penetration Depth (PD); 3) some basic generation metrics, including FID and Diversity. The FID quantifies the dissimilarity between the real and generated motions, while the diversity measures the variance of different motions. Additionally, we conduct a user study in which participants rated the gaze-motion consistency (GMC) and the interactions naturalness (IN) on a five-point scale. Higher scores reflect better motion generation quality.

B. Implementation Details

GHO-Diffusion is built upon a transformer encoder, following the approach of [50], with 1000 denoising steps. We utilize a single NVIDIA GeForce RTX 4090 GPU for training. To simplify the model, we randomly sample 500 points from the surface of the object. The batch size is set to 128, with a learning rate of $1e-5$. The latent dimension is uniformly set to 128 for object diffusion and 256 for hand diffusion. For stage-1, the hyperparameters are set as $\lambda_\alpha = 10$, $\lambda_t = 30$, $\lambda_v = 10$, $\lambda_s = 1$. For stage-2, the hyperparameters are set as $\lambda_\beta = 100$, $\lambda_b = 100$. For HOI-Manifold guidance, we set $\lambda_k = 100$, $\lambda_c = 1000$, $\lambda_p = 100$ and guidance rate $w = 0.99$. We designed the hyperparameters based on our expertise to balance the weights of each loss component, ensuring they remain within appropriate magnitudes for optimal performance.

C. Baseline Design and Comparison

Our method is the first to generate both hand and object motions from gaze data, and there are no direct methods available for comparison. Here are some related baselines.

1) *Text2HOI**: The most closely related state-of-the-art work is Text2HOI [47], which generates a contact map conditioned on texts and then combines it to produce hand-object motions. Due to the observation of the relationship

between gaze and contact, we adapt the approach by replacing the text encoder with our spatial-temporal gaze encoding to generate the contact map. The architecture of the models, as well as the training loss functions, are consistent with those described in the original Text2HOI paper. Since the original authors only released the testing code and did not provide the full training code, we reproduced the training process based on the methodology described in the Text2HOI paper. The definition of the loss function was also referenced from the Contact2Grasp [34] and InterGen [54] code mentioned in Text2HOI.

2) *MDM**: We also employed MDM [50] as a baseline, as it is a classic benchmark for diffusion-based motion generation. We replace the condition encoder of MDM [50] with our spatial-temporal gaze encoding and introduce three additional loss functions to better align with our task requirements:

$$\mathcal{L}_{MDM^*} = \lambda_\gamma \mathcal{L}_{simple} + \lambda_o \mathcal{L}_{obj} + \lambda_h \mathcal{L}_{hand} + \lambda_f \mathcal{L}_{offset}, \quad (21)$$

where \mathcal{L}_{obj} and \mathcal{L}_{hand} independently constraint the object and hand translation, while \mathcal{L}_{offset} is defined to constraint the offset between object center points and hand wrist joints.

$$\mathcal{L}_{obj} = \sum_{i=1}^L \|\mathbf{T}_o^i - \hat{\mathbf{T}}_o^i\|_2, \quad (22)$$

$$\mathcal{L}_{hand} = \sum_{i=1}^L \|\mathbf{T}_h^i - \hat{\mathbf{T}}_h^i\|_2, \quad (23)$$

$$\mathcal{L}_{offset} = \sum_{i=1}^L \|(\mathbf{T}_h^i - \mathbf{T}_o^i) - (\hat{\mathbf{T}}_h^i - \hat{\mathbf{T}}_o^i)\|_2, \quad (24)$$

where the hyperparameters are set as $\lambda_\gamma = 20$, $\lambda_o = 20$, $\lambda_h = 20$, and $\lambda_f = 30$.

3) *OMOMO**: Object-Conditioned Hand Motion Synthesis is a key component of our method. Although there is no direct baseline for our entire task, OMOMO [42] is closely related to this aspect, so we compare our approach with OMOMO, using our fully designed stage-1 to acquire the object motions.

TABLE IV
QUANTITATIVE COMPARISON ON SEEN OBJECTS AND UNSEEN OBJECTS.

Methods	Seen Objects							Unseen Objects						
	MPVPE ↓	FOL ↓	MPJPE ↓	CF↑	PD ↓	GMC↑	IN↑	MPVPE ↓	FOL ↓	MPJPE ↓	CF↑	PD ↓	GMC↑	IN↑
MDM*	147.5	214.4	165.8	42.30	2.17	4.05	3.55	146.6	231.8	166.8	68.19	2.62	3.40	3.35
Text2HOI*	316.7	324.6	267.0	46.00	1.97	3.00	2.70	327.3	327.8	255.6	63.44	2.66	2.85	2.50
OMOMO*	-	-	157.2	52.00	1.95	4.30	4.2	-	-	163.3	65.57	2.65	4.00	3.60
Ours	113.1	133.3	146.6	59.28	1.92	4.90	4.75	118.7	150.2	144.3	70.55	2.61	4.70	4.55

TABLE V
ABLATION ON GAZE REPRESENTATION AND ENCODING. OURS- MEANS OUR FULL METHOD WITHOUT MOTION SELECTION FOR A FAIR COMPARISON.

	MPVPE↓	FOL↓	GMC↑
gaze ray	126.7	189.2	3.95
w/o spatial	128.4	193.8	3.90
w/o temporal	119.3	163.4	4.15
Ours-	117.9	157.6	4.25

Quantitative and qualitative results are shown in Table III and Figure 6, demonstrating that our method significantly outperforms the other baselines across all metrics and visualizations. The MPVPE and FOL metrics for OMOMO* are marked with “-” because OMOMO* only includes comparisons for stage-2 and directly uses our stage-1 results. Therefore, these two metrics are excluded from the comparison.

D. Ablation Study

1) *Results on Seen and Unseen Objects:* To evaluate the model’s generalization capabilities and mitigate potential overfitting to object-specific traits, the test set is carefully designed to include a majority of objects not present in the training set. Specifically, among the 275 test sequences, 215 feature entirely new objects unseen during training, while 60 involve objects encountered during training but are paired with more complex interaction tasks, such as assembling or playing chess. These challenging tasks introduce additional errors in hand pose generation, providing a rigorous test of the method’s robustness and adaptability across varying levels of interaction complexity. As shown in Figure 6 and Table IV, our method outperforms others on both seen and unseen objects, delivering motions that are natural and plausible, while closely aligning with the underlying information encoded in the gaze data. The results demonstrate that our method exhibits superior performance on both seen and unseen objects.

2) *Gaze Representation and Encoding:* As the first method to use gaze as a condition for motion generation, we explore the effectiveness of different gaze representations and spatial-temporal feature encoding. The results are in Table V. The results show that our method effectively captures both spatial and temporal features, enabling efficient extraction of the rich information encoded in gaze data.

3) *HOI-Manifold Guidance:* The guidance-free method suffers from problems like lack of contact and penetration, while the naïve guidance strategy partially mitigates these problems but introduces motion distortions, compromising the naturalness of the results. In contrast, our HOI-Manifold

TABLE VI
ABLATION ON DIFFERENT GUIDANCE STRATEGIES. OURS- MEANS OUR FULL METHOD WITHOUT MOTION SELECTION FOR A FAIR COMPARISON.

	MPJPE ↓	CF↑	PD ↓	IN↑
w/o guidance	155.3	64.65	2.61	3.9
naïve guidance	156.8	63.66	2.44	3.5
Ours-	154.3	65.77	2.51	4.45

Guidance strategy strikes a balance between these challenges, achieving superior outcomes as shown in Table VI.

4) *Motion Selection via Gaze-interaction Consistency Score:* Table VII demonstrates the effectiveness of our designed gaze-interaction consistency score, showing that motions selected by this score are more closely aligned with the information implied in the gaze data.

VI. TASK: HAND-OBJECT MOTION RECONSTRUCTION

Due to our rigorous data collection process and the precise alignment achieved across multiple coordinate systems, the GazeHOI dataset ensures that the 3D hand-object data is exceptionally well-aligned with the corresponding image data. This high level of alignment makes GazeHOI an ideal resource for tackling complex hand-object reconstruction tasks, as it provides a seamless integration between 3D spatial information and visual cues from images.

A. Task Definition

Given a video of hand-object interactions and the object’s mesh, the task goal is to reconstruct continuous, smooth, and natural hand-object interaction motions for each frame.

B. Data Split and Metrics

The data utilized in the experiment comprises 12 side views from our complete dataset, totaling 3.0M images. We divide the data by subjects, 8 subjects for training, 1 for evaluation, and 1 for testing. To measure hand-object reconstruction quality, we compute Mean Relative-Root Position Error (MRRPE) for left-to-right and right-to-object interactions and Mean Per Joint Position Error (MPJPE) in local space. Additionally, following [21], we evaluate errors in object poses through a success rate metric that is the percentage of predicted object vertices with an L2 error to the ground truth which is less than 5% of the object’s diameter.

C. Baselines and Results

To validate the quality of our dataset, substantiate its utility beyond synthesis tasks for reconstruction tasks, and establish a benchmark for later works, we select two Hand-Object Motion Reconstruction baselines consistent with our

TABLE VII
ABLATION ON MOTION SELECTION VIA GAZE-INTERACTION CONSISTENCY SCORE.

	MPVPE↓	FOL↓	MPJPE↓	CF↑	PD↓	FID↓	GMC↑	IN↑
w/o select	117.9	157.6	154.3	65.77	2.51	0.048	4.25	4.45
w/o global	117.9	156.4	145.7	67.89	2.47	0.045	4.40	4.55
w/o local	117.5	148.9	149.8	65.96	2.50	0.046	4.35	4.45
Ours	117.4	146.5	144.8	68.10	2.46	0.044	4.75	4.60

TABLE VIII
PERFORMANCE OF BASELINE MODELS ON THE HAND-OBJECT MOTION RECONSTRUCTION TASK WITHIN OUR GAZEHOI DATASET

Splits	Methods	MRRPE↓	MPJPE↓	Success Rate↑
Validation	ArcticNet-SF [21]	111.2/43.5	23.7	20.3
	ArcticNet-LSTM [21]	114.9/45.2	24.0	22.5
	Keypoint Transformer [55]	108.9/42.6	32.6	28.4
Test	ArcticNet-SF [21]	65.1/42.6	22.8	29.7
	ArcticNet-LSTM [21]	68.9/42.4	23.1	33.0
	Keypoint Transformer [55]	111.4/42.5	27.6	44.9

dataset setting. The first baseline ArcticNet [21] is a naive model that obtains hand and object motions separately. It has two versions: an image-based model (ArcticNet-SF) and a video-based model (ArcticNet-LSTM) that allows reasoning of hand and object motions. Another one Keypoint Transformer [55] is an image-based model that performs well on several challenging datasets, including InterHand2.6M [56], HO-3D [16] and H2O-3D [55], through solving joint identification. We evaluate its performance on the results of each frame like the ArcticNet-SF. Table VIII shows the quantitative results of our baselines.

VII. CONCLUSION

We have proposed a novel task of Gaze-guided Hand-Object Interaction Synthesis and introduced a new dataset GazeHOI to support this task. GazeHOI is the first dataset to capture simultaneous 3D modeling of gaze, hand, and object interactions. To address this task, we proposed a stacked gaze-guided hand-object interaction diffusion model, named GHO-Diffusion, and further introduced HOI-Manifold Guidance in the sampling stage to force the guidance within the data manifold. We further exploited the consistency between gaze-contact maps and gaze-interaction trajectories to refine the generated motions. The extensive experimental results have validated the effectiveness of our method and the unique contributions of our dataset. While GazeHOI captures a diverse range of objects and tasks, it does not include articulated objects, which could present unique interaction challenges. In future work, we aim to extend this research by incorporating additional modalities, such as text descriptions and electromyography data to generate more context-aware interactive motions.

REFERENCES

- [1] W. X. Schneider, "Vam: A neuro-cognitive model for visual attention control of segmentation, object recognition, and space-based motor action," *Visual Cognition*, vol. 2, no. 2-3, pp. 331–376, 1995. [Online]. Available: <https://doi.org/10.1080/13506289508401737>
- [2] J. Gottlieb, P.-Y. Oudeyer, M. Lopes, and A. Baranes, "Information-seeking, curiosity, and attention: computational and neural mechanisms," *Trends in cognitive sciences*, vol. 17, no. 11, pp. 585–593, 2013.
- [3] L. Desanghere and J. J. Marotta, "The influence of object shape and center of mass on grasp and gaze," *Frontiers in psychology*, vol. 6, p. 1537, 2015.
- [4] A. A. Abdelrahman, T. Hempel, A. Khalifa, A. Al-Hamadi, and L. Dinges, "L2cs-net: Fine-grained gaze estimation in unconstrained environments," in *2023 8th International Conference on Frontiers of Signal Processing (ICFSP)*. IEEE, 2023, pp. 98–102.
- [5] Y. Guan, Z. Chen, W. Zeng, Z. Cao, and Y. Xiao, "End-to-end video gaze estimation via capturing head-face-eye spatial-temporal interaction context," *IEEE Signal Processing Letters*, vol. 30, pp. 1687–1691, 2023.
- [6] R. Kothari, S. De Mello, U. Iqbal, W. Byeon, S. Park, and J. Kautz, "Weakly-supervised physically unconstrained gaze estimation," in *Proceedings of the IEEE/CVF Conference on Computer Vision and Pattern Recognition*, 2021, pp. 9980–9989.
- [7] T. Fischer, H. J. Chang, and Y. Demiris, "Rt-gene: Real-time eye gaze estimation in natural environments," in *Proceedings of the European conference on computer vision (ECCV)*, 2018, pp. 334–352.
- [8] K. Lv, H. Sheng, Z. Xiong, W. Li, and L. Zheng, "Improving driver gaze prediction with reinforced attention," *IEEE Transactions on Multimedia*, vol. 23, pp. 4198–4207, 2021.
- [9] S. Zhang, Y. Tian, Y. Zhang, M. Tian, and Y. Huang, "Domain-consistent and uncertainty-aware network for generalizable gaze estimation," *IEEE Transactions on Multimedia*, vol. 26, pp. 6996–7011, 2024.
- [10] J. Lou, H. Lin, P. Young, R. White, Z. Yang, S. C. Sheldermine, D. Marshall, E. Spezi, M. Palombo, and H. Liu, "Predicting radiologists' gaze with computational saliency models in mammogram reading," *IEEE Transactions on Multimedia*, vol. 26, pp. 256–269, 2024.
- [11] P. Kratzer, S. Bihlmaier, N. B. Midlagajni, R. Prakash, M. Toussaint, and J. Mainprice, "Mogaze: A dataset of full-body motions that includes workspace geometry and eye-gaze," *IEEE Robotics and Automation Letters*, vol. 6, no. 2, pp. 367–373, 2020.
- [12] Y. Zheng, Y. Yang, K. Mo, J. Li, T. Yu, Y. Liu, C. K. Liu, and L. J. Guibas, "Gimo: Gaze-informed human motion prediction in context," in *European Conference on Computer Vision*. Springer, 2022, pp. 676–694.
- [13] J. DelPreto, C. Liu, Y. Luo, M. Foshey, Y. Li, A. Torralba, W. Matusik, and D. Rus, "Actionsense: A multimodal dataset and recording framework for human activities using wearable sensors in a kitchen environment," *Advances in Neural Information Processing Systems*, vol. 35, pp. 13 800–13 813, 2022.
- [14] F. Ragusa, A. Furnari, S. Livatino, and G. M. Farinella, "The meccano dataset: Understanding human-object interactions from egocentric videos in an industrial-like domain," in *Proceedings of the IEEE/CVF Winter Conference on Applications of Computer Vision*, 2021, pp. 1569–1578.
- [15] M. Eren Akbiyik, N. Savov, D. Pani Paudel, N. Popovic, C. Vater, O. Hilliges, L. Van Gool, and X. Wang, "G-memp: Gaze-enhanced multimodal ego-motion prediction in driving," *arXiv e-prints*, pp. arXiv-2312, 2023.
- [16] S. Hampali, M. Rad, M. Oberweger, and V. Lepetit, "Honnotate: A method for 3d annotation of hand and object poses," in *Proceedings of the IEEE/CVF Conference on Computer Vision and Pattern Recognition (CVPR)*, June 2020.

- [17] Y.-W. Chao, W. Yang, Y. Xiang, P. Molchanov, A. Handa, J. Tremblay, Y. S. Narang, K. Van Wyk, U. Iqbal, S. Birchfield, J. Kautz, and D. Fox, "Dexycb: A benchmark for capturing hand grasping of objects," in *Proceedings of the IEEE/CVF Conference on Computer Vision and Pattern Recognition (CVPR)*, June 2021, pp. 9044–9053.
- [18] T. Kwon, B. Tekin, J. Stühmer, F. Bogo, and M. Pollefeys, "H2o: Two hands manipulating objects for first person interaction recognition," in *Proceedings of the IEEE/CVF International Conference on Computer Vision (ICCV)*, October 2021, pp. 10 138–10 148.
- [19] L. Yang, K. Li, X. Zhan, F. Wu, A. Xu, L. Liu, and C. Lu, "Oakink: A large-scale knowledge repository for understanding hand-object interaction," in *Proceedings of the IEEE/CVF Conference on Computer Vision and Pattern Recognition (CVPR)*, June 2022, pp. 20 953–20 962.
- [20] Y. Liu, Y. Liu, C. Jiang, K. Lyu, W. Wan, H. Shen, B. Liang, Z. Fu, H. Wang, and L. Yi, "Hoi4d: A 4d egocentric dataset for category-level human-object interaction," in *Proceedings of the IEEE/CVF Conference on Computer Vision and Pattern Recognition (CVPR)*, June 2022, pp. 21 013–21 022.
- [21] Z. Fan, O. Taheri, D. Tzionas, M. Kocabas, M. Kaufmann, M. J. Black, and O. Hilliges, "Arctic: A dataset for dexterous bimanual hand-object manipulation," in *Proceedings of the IEEE/CVF Conference on Computer Vision and Pattern Recognition (CVPR)*, June 2023, pp. 12 943–12 954.
- [22] Y. Liu, H. Yang, X. Si, L. Liu, Z. Li, Y. Zhang, Y. Liu, and L. Yi, "Taco: Benchmarking generalizable bimanual tool-action-object understanding," *arXiv preprint arXiv:2401.08399*, 2024.
- [23] J. Zhang, H. Luo, H. Yang, X. Xu, Q. Wu, Y. Shi, J. Yu, L. Xu, and J. Wang, "Neuraldome: A neural modeling pipeline on multi-view human-object interactions," in *Proceedings of the IEEE/CVF Conference on Computer Vision and Pattern Recognition (CVPR)*, June 2023, pp. 8834–8845.
- [24] C. Zhao, J. Zhang, J. Du, Z. Shan, J. Wang, J. Yu, J. Wang, and L. Xu, "I'm hoi: Inertia-aware monocular capture of 3d human-object interactions," *arXiv preprint arXiv:2312.08869*, 2023.
- [25] X. Zhan, L. Yang, Y. Zhao, K. Mao, H. Xu, Z. Lin, K. Li, and C. Lu, "Oakink2: A dataset of bimanual hands-object manipulation in complex task completion," in *Proceedings of the IEEE/CVF Conference on Computer Vision and Pattern Recognition*, 2024, pp. 445–456.
- [26] C. Lugaresi, J. Tang, H. Nash, C. McClanahan, E. Uboweja, M. Hays, F. Zhang, C. Chang, M. G. Yong, J. Lee, W. Chang, W. Hua, M. Georg, and M. Grundmann, "Mediapipe: A framework for building perception pipelines," *CoRR*, vol. abs/1906.08172, 2019. [Online]. Available: <http://arxiv.org/abs/1906.08172>
- [27] S.-Y. Chen, Y.-K. Lai, S. hong Xia, P. L. Rosin, and L. Gao, "3d face reconstruction and gaze tracking in the hmd for virtual interaction," *IEEE Transactions on Multimedia*, vol. 25, pp. 3166–3179, 2023.
- [28] X. Wang, T. Kwon, M. Rad, B. Pan, I. Chakraborty, S. Andrist, D. Bohus, A. Feniello, B. Tekin, F. V. Frujeri *et al.*, "Holoassist: an egocentric human interaction dataset for interactive ai assistants in the real world," in *Proceedings of the IEEE/CVF International Conference on Computer Vision*, 2023, pp. 20 270–20 281.
- [29] X. Pan, N. Charron, Y. Yang, S. Peters, T. Whelan, C. Kong, O. Parkhi, R. Newcombe, and Y. C. Ren, "Aria digital twin: A new benchmark dataset for egocentric 3d machine perception," in *Proceedings of the IEEE/CVF International Conference on Computer Vision*, 2023, pp. 20 133–20 143.
- [30] S. Zhang, Q. Ma, Y. Zhang, Z. Qian, T. Kwon, M. Pollefeys, F. Bogo, and S. Tang, "Egobody: Human body shape and motion of interacting people from head-mounted devices," in *European Conference on Computer Vision*. Springer, 2022, pp. 180–200.
- [31] M. Liu, S. Tang, Y. Li, and J. M. Rehg, "Forecasting human-object interaction: joint prediction of motor attention and actions in first person video," in *Computer Vision—ECCV 2020: 16th European Conference, Glasgow, UK, August 23–28, 2020, Proceedings, Part I 16*. Springer, 2020, pp. 704–721.
- [32] H. Yan, Z. Hu, S. Schmitt, and A. Bulling, "Gazemodiff: Gaze-guided diffusion model for stochastic human motion prediction," *arXiv preprint arXiv:2312.12090*, 2023.
- [33] Z. Hu, S. Schmitt, D. Haeuffle, and A. Bulling, "Gazemotion: Gaze-guided human motion forecasting," *arXiv preprint arXiv:2403.09885*, 2024.
- [34] H. Li, X. Lin, Y. Zhou, X. Li, Y. Huo, J. Chen, and Q. Ye, "Contact2grasp: 3d grasp synthesis via hand-object contact constraint," *arXiv preprint arXiv:2210.09245*, 2022.
- [35] H. Jiang, S. Liu, J. Wang, and X. Wang, "Hand-object contact consistency reasoning for human grasps generation," in *Proceedings of the IEEE/CVF International Conference on Computer Vision*, 2021, pp. 11 107–11 116.
- [36] S. Liu, Y. Zhou, J. Yang, S. Gupta, and S. Wang, "Contactgen: Generative contact modeling for grasp generation," in *Proceedings of the IEEE/CVF International Conference on Computer Vision*, 2023, pp. 20 609–20 620.
- [37] P. Grady, C. Tang, C. D. Twigg, M. Vo, S. Brahmabhatt, and C. C. Kemp, "Contactopt: Optimizing contact to improve grasps," in *Proceedings of the IEEE/CVF Conference on Computer Vision and Pattern Recognition*, 2021, pp. 1471–1481.
- [38] H. Zhang, Y. Ye, T. Shiratori, and T. Komura, "Manipnet: neural manipulation synthesis with a hand-object spatial representation," *ACM Transactions on Graphics (ToG)*, vol. 40, no. 4, pp. 1–14, 2021.
- [39] K. Karunratanakul, K. Preechakul, S. Suwajanakorn, and S. Tang, "Guided motion diffusion for controllable human motion synthesis," in *Proceedings of the IEEE/CVF International Conference on Computer Vision*, 2023, pp. 2151–2162.
- [40] O. Taheri, Y. Zhou, D. Tzionas, Y. Zhou, D. Ceylan, S. Pirk, and M. J. Black, "Grip: Generating interaction poses using spatial cues and latent consistency," in *2024 International Conference on 3D Vision (3DV)*. IEEE, 2024, pp. 933–943.
- [41] K. Zhou, B. L. Bhatnagar, J. E. Lenssen, and G. Pons-Moll, "Gears: Local geometry-aware hand-object interaction synthesis," in *Proceedings of the IEEE/CVF Conference on Computer Vision and Pattern Recognition*, 2024, pp. 20 634–20 643.
- [42] J. Li, J. Wu, and C. K. Liu, "Object motion guided human motion synthesis," *ACM Transactions on Graphics (TOG)*, vol. 42, no. 6, pp. 1–11, 2023.
- [43] J. Zheng, Q. Zheng, L. Fang, Y. Liu, and L. Yi, "Cams: Canonicalized manipulation spaces for category-level functional hand-object manipulation synthesis," in *Proceedings of the IEEE/CVF Conference on Computer Vision and Pattern Recognition*, 2023, pp. 585–594.
- [44] S. Christen, M. Kocabas, E. Aksan, J. Hwangbo, J. Song, and O. Hilliges, "D-grasp: Physically plausible dynamic grasp synthesis for hand-object interactions," in *Proceedings of the IEEE/CVF Conference on Computer Vision and Pattern Recognition*, 2022, pp. 20 577–20 586.
- [45] O. Taheri, V. Choutas, M. J. Black, and D. Tzionas, "Goal: Generating 4d whole-body motion for hand-object grasping," in *Proceedings of the IEEE/CVF Conference on Computer Vision and Pattern Recognition*, 2022, pp. 13 263–13 273.
- [46] A. Ghosh, R. Dabral, V. Golyanik, C. Theobalt, and P. Slusallek, "Imos: Intent-driven full-body motion synthesis for human-object interactions," 2023.
- [47] J. Cha, J. Kim, J. S. Yoon, and S. Baek, "Text2hoi: Text-guided 3d motion generation for hand-object interaction," in *Proceedings of the IEEE/CVF Conference on Computer Vision and Pattern Recognition*, 2024, pp. 1577–1585.
- [48] S. Christen, S. Hampali, F. Sener, E. Remelli, T. Hodan, E. Sauser, S. Ma, and B. Tekin, "Diffh2o: Diffusion-based synthesis of hand-object interactions from textual descriptions," *arXiv:2403.17827*, 2024.
- [49] J. Romero, D. Tzionas, and M. J. Black, "Embodied hands: Modeling and capturing hands and bodies together," *ACM Transactions on Graphics (Proc. SIGGRAPH Asia)*, vol. 36, no. 6, Nov. 2017.
- [50] G. Tevet, S. Raab, B. Gordon, Y. Shafir, D. Cohen-Or, and A. H. Bermano, "Human motion diffusion model," *arXiv preprint arXiv:2209.14916*, 2022.
- [51] C. R. Qi, L. Yi, H. Su, and L. J. Guibas, "Pointnet++: Deep hierarchical feature learning on point sets in a metric space," *Advances in neural information processing systems*, vol. 30, 2017.
- [52] L. Yang, S. Ding, Y. Cai, J. Yu, J. Wang, and Y. Shi, "Guidance with spherical gaussian constraint for conditional diffusion," *arXiv preprint arXiv:2402.03201*, 2024.
- [53] A. Seshan, "Using machine learning to augment dynamic time warping based signal classification," *arXiv preprint arXiv:2206.07200*, 2022.
- [54] H. Liang, W. Zhang, W. Li, J. Yu, and L. Xu, "Intergen: Diffusion-based multi-human motion generation under complex interactions," *International Journal of Computer Vision*, pp. 1–21, 2024.
- [55] S. Hampali, S. D. Sarkar, M. Rad, and V. Lepetit, "Keypoint transformer: Solving joint identification in challenging hands and object interactions for accurate 3d pose estimation," in *2022 IEEE/CVF Conference on Computer Vision and Pattern Recognition (CVPR)*, 2022, pp. 11 080–11 090.
- [56] G. Moon, S.-I. Yu, H. Wen, T. Shiratori, and K. M. Lee, "Interhand2.6m: A dataset and baseline for 3d interacting hand pose estimation from a single rgb image," in *Computer Vision—ECCV 2020: 16th European Conference, Glasgow, UK, August 23–28, 2020, Proceedings, Part XX 16*. Springer, 2020, pp. 548–564.